https://doi.org/10.5194/egusphere-2026-2779
Preprint. Discussion started: 10 June 2026

Causes and mitigation of U-Pb fractionation during LA-ICPMS analyses of zircon using nanosecond excimer laser systems

Donald W. Davis and Heriberto Rochin-Banaga

Earth Sciences Department, University of Toronto, 22 Ursula Franklin St., ON, M5S 3B1, Canada

Correspondence to: D. W. Davis (don.davis@utoronto.ca)

Abstract. This work investigates the causes of measurement biases in U-Pb dating of zircon by laser ablation inductively coupled mass spectrometry (LA-ICPMS) and possible methods for correction. Plasma-induced biases include oxidative loss of U, which is normally minimized by restricting nebulizer Ar flow at the cost of lower sensitivity, mass bias and ionization efficiency, which together normally produce a negative bias of several tens of percent for $^{206}Pb/^{238}U$. There is also an ablation bias due to the relative volatility of Pb, which depends to some extent on the structural state of the zircon. We suggest that oxidation of elements in the plasma is caused by turbulent entrainment of oxygen from the surrounding air and point out a flaw in the design of some movable two-stage ablation chambers that can result in variable degrees of oxidation as position is changed. Measurements of NIST glass and zircon include significant ablation bias even when scanned. The main cause of increasing $^{206}Pb/^{238}U$ ablation bias seen in zircon and other minerals appears to be sequestration of Pb-depleted melt in fallback and along the sides of the pit. Integrated signal profiles measured using laser pulses at 0.2 Hz combined with modelling of U/Pb fractionation suggest that the earliest Pb/U measurements (first 10 pulses) are affected by decreasing fractionation from a melt pool as it becomes increasingly depleted in Pb. This trend is opposed by deposition of depleted material as fallback, which dominates signal loss for the first 10 pulses but rapidly decreases. The fractionation sequence from the first 10 or so pulses is therefore chaotic. Ratios from the following 50 or so pulses show an approximately linear increase in fractionation. Normalized data from these pulses give trends with higher intercepts and lower slopes for standards with higher radiation damage during the same session. Fractionation and signal decay subsequently rise more slowly but remain linear, probably because fractionation is dominated by deposition in the deepening pit. An ablation fractionation model is proposed based on the drop in measured signal but this cannot be used to estimate accurate bias-free $^{206}Pb/^{238}U$ ratios because of the number of unconstrained parameters. The best approach for calibrating against an unknown is a direct comparison of all or part of the standard ratio profile with the sample profile after multiplication by a calibration factor. The factor that

https://doi.org/10.5194/egusphere-2026-2779
Preprint. Discussion started: 10 June 2026

results in the best fit should represent a ratio of unbiased $^{206}Pb/^{238}U$ between standard and sample. Software is included to process and calibrate data. Data from Precambrian zircon with well-established $^{207}Pb/^{206}Pb$ ages suggest that radiation damage below the metamict state results in little bias to discordance. Reverse discordance from metamict zircon appears to be approximately proportional to U concentration. Increased accuracy of $^{206}Pb/^{238}U$ ages using nanosecond laser systems can most likely be achieved through design improvements rather than data processing. Sensitivity should be increased and ablation bias decreased by reducing the volume in the sampling cup to minimize fallback. Plasma cooling in a flow of N_2 gas from a liquid nitrogen dewar should enable increased sensitivity without oxidation of U. The use of H_2, instead of He as a carrier gas should reduce fallback and cost but would require design changes to prevent exposure to the plasma before complete venting of O_2 from the ablation chamber.

1. Introduction

Laser ablation inductively coupled plasma mass spectrometry (LA-ICPMS) has proved to be a powerful analytical approach for U-Pb geochronology because of the speed and scale of analyses (less than 1 minute at a scale of tens of microns in situ). It has led to a large increase in the number of publications on dating zircon, as well as applications to hydrogenic and biogenic minerals like calcite and phosphate. The analytical precision is limited to about 1% for a single analysis with quadrupole mass analyzers but can be better for rapid switching or multi-collector sector instruments and the rapidity of analyses makes it relatively easy to generate large amounts of data that can be averaged.

Because of the complexity of the analytical processes, LA-ICPMS is often treated like a ‘black box’ by users (including the authors). This may lead to the adoption of empirical analytical protocols whose basis is poorly understood. A significant problem compared to isotope dilution is assuring the accuracy of data, especially where ages depend on Pb/U measurement such as samples younger than Mesoproterozoic (e.g. zircon) or samples that contain significant common Pb (e.g. calcite). This is because measurement biases for $^{206}Pb/^{238}U$ ratios are normally high and must be corrected, usually by measuring standards with known ratios and assuming the same ablation bias as for the sample.

The most significant sources of Pb/U measurement bias are mass fractionation, ionization efficiency, oxidative loss of U and ablation bias. The first three occur in the plasma while the fourth is a result of interaction of the laser with the sample. A common procedure in analyzing calcites and phosphates is to correct for the first three biases using a glass standard such as NIST612 or NIST614 (Jochum et al., 2011) but these are also affected by ablation bias, which can only be corrected using a ‘matrix-matched’ standard, which is usually the same mineral

https://doi.org/10.5194/egusphere-2026-2779
Preprint. Discussion started: 10 June 2026

as the sample but with a relatively precisely known age measured by isotope dilution thermal ionization mass spectrometry (ID-TIMS). There can be problems with this that compromise accuracy even when measurements produce precise results. Glass standards are subject to significant Pb/U ablation biases (see below). Measuring a standard of similar mineralogy to the sample may not adequately correct for ablation bias for samples such as calcite, which can have quite variable compositions, or zircon, which can have variable states of crystallinity due to radiation damage.

A series of experiments, interpretations and suggestions are presented to better understand the causes of Pb/U bias in zircon during LA-ICPMS measurements and suggest ways that these and other sources of bias can be mitigated to improve accuracy of U-Pb ages. Working hypotheses will be advanced to explain results of measurements. Even if these explanations are not all strictly valid, they may provide a starting point for understanding the causes of bias and how to accurately correct it. We hope that our observations and arguments will at least provide some insight to the community and inspire further efforts.

2. Instrumentation and Materials

U–Pb isotopic analyses were conducted at the University of Toronto using an Agilent 7900 ICPMS and an NWR193 excimer laser ablation system. The laser was normally run at a frequency of either 10 Hz or 0.5 Hz with fluence of 3.5 mj/cm^2. Beam diameter was varied as noted for the experiments described below. Initial tuning and measurement of plasma characteristics were carried out using NIST610 ablated along scan lines. The He flow rate was set at 1000 ml/min and nebulizer Ar flow rate was adjusted to give ThO/Th of 0.5% or less, except where otherwise noted. All data were measured in the same lab under variable specified conditions.

Primary standards include NIST610 and NIST612 glasses. Zircon standards include Keuhl Lake (KL) from a zircon megacryst in the same deposit as standard 91500 (1065 Ma; Caulfield et al., 2025; Wiedenbeck et al., 1995; Royal Ontario Museum object number ROMESM16401), DD91-1 zircon, a relatively high-U (300 ppm) zoned 2682 ± 1.2 Ma zircon (Davis, 2002) and DD85-17, a relatively low U (100 ppm) zoned 3002 ± 3 Ma zircon (Tomlinsen et al., 2003). KL is mostly unzoned and has a very low degree of radiation damage as revealed by Raman scattering (Das and Davis, 2010).

https://doi.org/10.5194/egusphere-2026-2779
Preprint. Discussion started: 10 June 2026

3. Results and Discussion: Sources of U-Pb bias

3.1 Plasma-induced biases

3.1.1 U Oxidation loss

Unless carefully controlled, oxidative loss of U can be a significant source of bias for the $^{206}Pb/^{238}U$ ratio. He gas carries the sample from the ablation chamber and is mixed with Ar in a tube (nebulizer chamber) before being injected into the plasma. The plasma is maintained within normal atmosphere and cooled by air flow around it. Fig. 1 shows the intensity of ^{206}Pb, ^{230}Th and ^{238}U as a function of oxygen in the plasma as measured by the ThO/Th ratio (Supplementary Data File 1). Measurements were made under normal laser operating conditions (30 microns, 10 Hz, 3.5 millijoules/cm^2) by laser scanning of NIST612. Intensity and oxide formation increase with sample gas flow into the plasma and are controlled by regulating the flow of the 'nebulizer' Ar added to the He. In making such plots it is important to deal with the problem that both sensitivity and ThO/Th change slowly but continually at the same gas flow even after hours of operation. This drift is usually in the direction of decreasing oxidation. Therefore, measurements were made by adjusting auxiliary Ar gas flow upwards in steps followed by the same steps downwards. The two results at the same intermediate steps are averaged for Figs 2-3 (Supplementary Data File 1). Fig. 1 shows that the sensitivity for all three elements increases rapidly with degree of oxidation. The increase slows when ThO/Th exceeds 1%. Above 2%, Th starts to decrease approximately linearly as does U at over 5% due to oxidative loss. Pb continues to increase although more slowly. Its sensitivity increases by a factor of about 4.5 over very low oxide conditions when ThO/Th approaches 50%. The relative degrees of oxidation may be related to the first and second ionization potentials of the elements. These are respectively 6.3 eV and 11.5 eV for Th, 6.2 eV and 14.7 eV for U and 7.4 eV and 15.0 eV for Pb. The potentials for Pb are significantly higher than the others, limiting oxidation. The first potential is lower for U than for Th but its second potential is significantly higher, apparently limiting its oxidation to below that of Th. These potentials may provide a basis for predicting molecular interferences (May and Wiedmeyer, 1998).

https://doi.org/10.5194/egusphere-2026-2779
Preprint. Discussion started: 10 June 2026

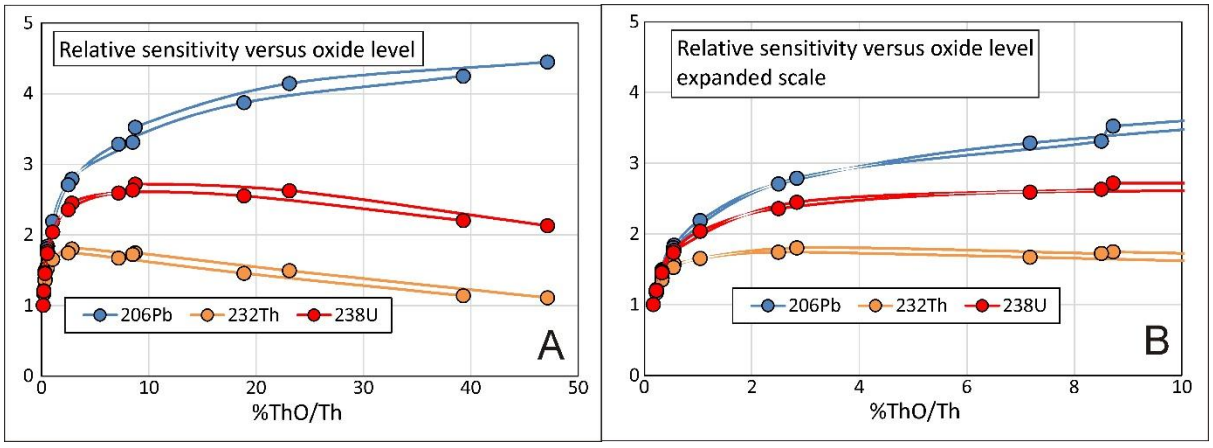

Figure 1: Sensitivity of Pb, U and Th as a function of oxidation in the plasma, as measured by ThO/Th. The vertical axis is the ratio of signal intensity to the intensity measured at the lowest oxide level. B is a blow-up of the left section of A. ThO/Th was varied by increasing Ar flow followed by a decrease over the same time period to average out the effect of secular decrease in ThO/Th when Ar flow is held constant.

Oxidation might result from entrainment of turbulent air into the plasma, which should increase with Ar gas flow rate. A higher flow rate projects the sample material closer to the orifice of the sampler cone, which may explain the increase in sensitivity (fewer charge-loss collisions of ions with neutral species having a lower ionization potential). Lowering depth of focus, which is the distance between the plasma torch and the sampler cone, has a similar effect to increasing the Ar flow. Adjusting the torch position closer to the sampler cone increases both sensitivity and ThO/Th.

For samples containing no or very minor sulphide, oxygen can be easily monitored using the $^{16}O^{18}O$ molecule since single oxygen isotope mass signals and even $^{40}Ar^{18}O+$ (Thompson et al., 2018) can be above the range for digital counting. Usually there is a minor increase in oxygen signal during ablation of zircon (but this may be significant with other minerals, see below). Baseline oxygen levels can be monitored along with other elements. The measured $^{16}O^{18}O^{+}$ signal is plotted against ThO/Th on Fig. 2. Interestingly, the relationship between the two is close to exponential (linear on a logarithmic scale) over the lower part of the range, with %ThO/Th increasing more slowly above about 5%. The $^{16}O^{18}O^{+}$ intensity should be the most direct indicator of oxidation potential and this is plotted against $^{206}Pb/^{238}U$ measurements on Fig. 3. The relationship appears to be approximately parabolic (the U-oxide equilibrium constant varies as the square of the oxygen concentration), as expected if U is in the +4 oxidation state (UO_2). The relationship may become more linear at higher O and the

https://doi.org/10.5194/egusphere-2026-2779
Preprint. Discussion started: 10 June 2026

slope is near-zero at zero concentration, although confirmation of this would require more data. The width of the best fit parabola narrows noticeably with plasma operating time, as does the measured $^{16}O^{18}O^{+}$ signal, suggesting that the temperature of the plasma spontaneously increases at a slow rate under constant operating conditions. The projection of the trend to an oxidation level of zero gives the best approximation of the $^{206}Pb/^{238}U$ unbiased by oxidation. It is, however, still biased by mass, ionization and ablation fractionation factors.

Despite the importance of high sensitivity it has long been recognized that oxidation levels should be kept low to reduce and stabilize Pb/U bias. Normally ThO/Th levels are kept at no more than 0.5% despite the cost in sensitivity. Continued decrease of this value leads to continued decrease in sensitivity so this represents a compromise.

Oxygen derived from the ablated sample, if significant, might induce variable U signal loss. There is only about a 5% increase in $^{16}O^{18}O^{+}$ levels during ablation of zircon, which should be negligible under normal operating conditions (see Fig. 3). A review of previous data sets from samples analysed in our lab shows that the difference in $^{16}O^{18}O^{+}$ levels between baseline and during ablation varies significantly depending on the material ablated. There is no detectable change for NIST-610 and monazite. However, $^{16}O^{18}O^{+}$ signal is larger and quite variable for scans of calcite standard WC1, which is a commonly used matrix matched standard in carbonate dating (Roberts et al., 2017), increasing up to factors of over 3 compared to zircon, whereas phosphates can show over an order of magnitude increase, which might induce significant loss of U due to oxidation during analysis of these minerals.

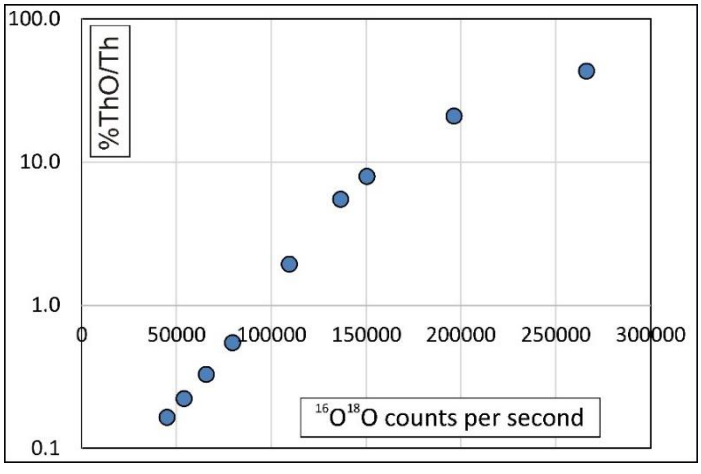

Figure 2: Measured baseline percent ThO/Th versus molecular oxygen. Note that scale is logarithmic.

https://doi.org/10.5194/egusphere-2026-2779
Preprint. Discussion started: 10 June 2026

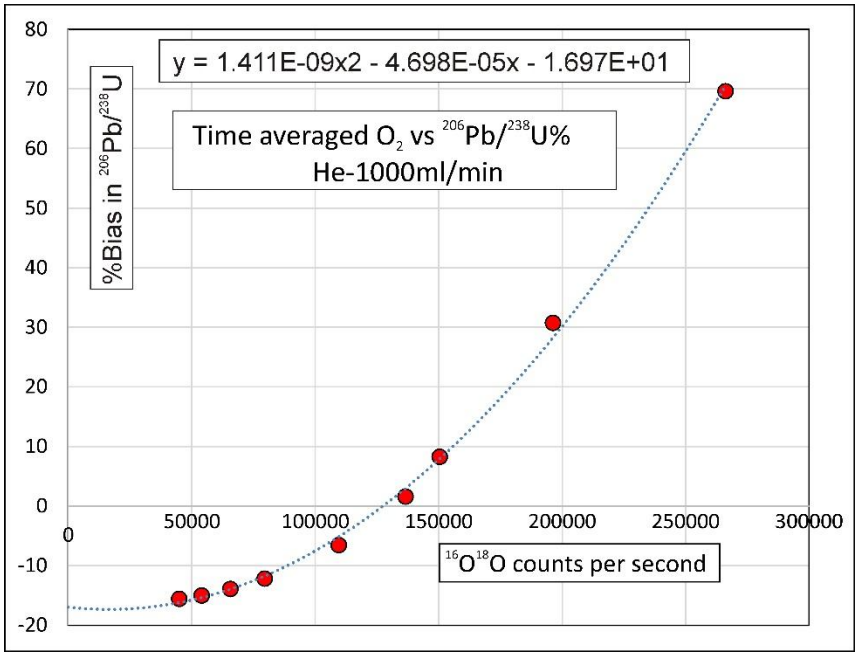

Figure 3: Measured percent difference between $^{206}Pb/^{238}U$ and the accepted value during ablation of NIST610 standard as a function of molecular oxygen in the plasma.

If high sensitivity is imperative, one possible approach to correcting oxide bias would be to conduct standard measurements at different oxygen values and extrapolate to the bias level at zero oxygen. The easiest way to do this is to change the He, rather than the auxiliary Ar, flow rate so that it can be done manually within a single acquisition file.

Because the plasma characteristics drift, it is necessary to take measurements at both increasing and decreasing He flow. This requires fitting a function of percent bias in measured $^{206}Pb/^{238}U$ versus $^{16}O^{18}O^{+}$ signal versus time and extrapolating it to zero $^{16}O^{18}O^{+}$ signal. Since there is a quadratic relationship between the variables this should require at least 3 measurements at different flow rates as well as extra measurements to correct for the time dependency. Correction can be done in Excel but the number of extra analyses required and inevitable expansion of errors makes it impractical in most cases.

A particularly insidious laboratory problem with oxidative bias is that it depends on the sample carrier gas flow rate into the plasma, which in some cases can be strongly dependent on position within the ablation chamber. Most 2-stage ablation systems consist of a rectangular chamber where polished samples and standards are placed. The chamber can be displaced in the X (left-right) and Y (in-out) direction to align the target area with the laser.

https://doi.org/10.5194/egusphere-2026-2779
Preprint. Discussion started: 10 June 2026

There is a plastic cylinder open at both ends within the chamber that is coaxial with the fixed laser beam and serves to channel the ablation plume. The chamber is pressurized with He gas, which is removed through a side hole near the top of the cylinder so the plume of ablated material will be efficiently conducted by the He out of the chamber and into the plasma by way of the Ar mixing (nebulizer) chamber. The He gas is normally extracted through a flexible tube that is connected to a stainless steel tube that remains fixed and must exit the movable chamber through a hole sealed by small O rings mounted over the tube. Such a design is not completely secure for preventing the flow of He around the rings and there can be significant loss of gas dependent on position, especially as the O rings age and stiffen. This results in a lowering of He flow into the plasma and a reduction in the oxidative bias, so it is important to keep ThO/Th low, and to minimize the X distance between samples and standards. It is useful to routinely monitor the $^{16}O^{18}O^{+}$ signal during analysis. This baseline will record any position-related variation.

Pb, U and Th do not seem to form nitrides so cooling the plasma torch in nitrogen, as opposed to drawing atmosphere around it, could mitigate loss due to U oxidation and maximize sensitivity. A limited flow of cold N_2 gas from a liquid nitrogen Dewar directed through a large cylinder surrounding the torch might cool it as effectively as a more rapid flow of room air. Such a configuration might also allow oxygen and carbon isotopic measurements to be performed by ICPMS. In addition, if the problem of increasing oxidation with time is related to increasing temperature of the plasma, this might be regulated by automatic adjustment of the power input to maintain the torch at a constant brightness.

3.1.2 Plasma bias: Mass fractionation and differential ionization

As shown below, calibration using a matrix-matched standard should correct both plasma and ablation bias. Nevertheless, it is important to understand the sources of all signal biases to optimize and improve measurement methods. For example, if ablation bias proved to be identical and therefore predictable for a large class of samples under similar laser conditions, knowing the plasma bias would eliminate the need to measure a standard. Bias produced by the plasma torch is therefore discussed below.

The plasma in an ICP torch is maintained by the transfer of radio frequency energy from a surrounding coil to electrons, which collide with and ionize Ar atoms that then also absorb enough energy to maintain a temperature of about 8000°K. Analyte injected into the plasma through the torch is rapidly volatilized and ionized. Levels of ionization depend on the ionization potential of the element but are much higher (>80% for most elements) than would be expected from the temperature of the plasma (Saha equation) due to collision with

https://doi.org/10.5194/egusphere-2026-2779
Preprint. Discussion started: 10 June 2026

energetic electrons in the plasma and with Ar ions, which will transfer charge to other elements having a lower ionization potential (Thomas, 2001).

In order to be detected, the ionized atom or molecule must make its way from the plasma at atmospheric pressure, through the orifice in the sampling cone, then through the orifice in the skimmer cone into a high vacuum region without losing its charge by collision with the wall or another species having a lower ionization energy. This is the reason that extraction efficiency is much less than 100%. The extraction efficiency is dependent on atomic or molecular weight, favoring heavier species. This, along with ionization efficiency, imposes a measurement bias of about minus 25-35% on the $^{206}Pb/^{238}U$ ratio (measured under low oxide conditions) which is the largest single source of bias.

Considering that elements have different ionization efficiencies, and assuming that there is neither loss nor gain of signal from isobaric molecules, the exponential fractionation law can be written:

$Rm/Rt = (I1/I2) * (M1/M2)^{\beta}$

Rm is the measured ratio of signals derived from mass M1 over M2 with Rt representing the fractionation-corrected (true) value and I1, I2 are ionization efficiencies for the two elements in the plasma. Since fractionation favours the heavy isotope if M1 < M2 then Rm < Rt making the exponential fractionation factor $\beta > 0$.

The ionization efficiency as a function of first ionization potentials (Φ) should form a reverse logistic curve where elements with the lowest first ionization potentials (<5 eV) are almost 100% ionized (see curve published by Agilent at https://www.agilent.com/cs/promotions/images/8030-img10.jpg):

$I = (1 - 1 / (1 + Exp(-K * (\Phi - \Phi m))))$

$= (Exp(-K*(\Phi - \Phi m))) / (1 + Exp(-K * (\Phi - \Phi m)))$

Where I is the fractional ionization of an element, Φ is its first ionization potential (usually in eV) of the element, Φm is the ionization potential that gives I = 0.5 (midpoint of the sigmoid curve) and K is a scale factor expressing the width of the curve. The curve is approximate since I should be 1 when $\Phi = 0$, which is only approximately true for the logistic function. Both ionization curve and mass discrimination depend on the temperature of the plasma.

An approximate average mass bias factor measured for $^{207}Pb/^{206}Pb$ is 1%/AMU, which implies a β value of 2.06. As seen below, a typical observed plasma bias for $^{206}Pb/^{238}U$ is roughly -30%. This implies a ratio of ionization efficiencies I206/I238 = 0.94, or that Pb should be ionized 6% less efficiently than U. Fitting a logistic curve to the ionization curve published by Agilent predicts ionization efficiencies of 99.3% for U and 93.2% for Pb, which accords well with observed biases. This curve will depend on plasma temperature as will the mass discrimination factor. If β were independent of mass, it would be possible to combine the two equations and solve

https://doi.org/10.5194/egusphere-2026-2779
Preprint. Discussion started: 10 June 2026

for β, Φm and K using proxy refractory elements. Unfortunately this effort was unsuccessful at least partly because β is mass-dependent. Its value for boron was found to be 0.72, which is very different from Pb.

An empirical approach would involve correcting plasma bias on $^{207}Pb/^{206}Pb$ and $^{206}Pb/^{238}U$ by measuring a primary standard. Horn et al., (2000) injected a calibrated nebulized solution of $^{205}Tl/^{238}U$ along with the ablation stream but did not obviously correct for different ionization efficiencies of Tl and Pb. The best approach might be to nebulize and inject a calibrated Pb/U solution between sample runs. The solution might have to also contain an appropriate concentration of Zr to match the composition of the sample.

The most convenient approach is to use laser scans but these are not free of ablation bias. Scans of NIST-610, 612 and 614 gave $^{206}Pb/^{238}U$ ratios biased relative to accepted values by -23.4%, -23.9% and -23.0%, respectively, whereas two scans of the Keuhl Lake zircon (KL) near the start and at the end the session gave biases of -27.6% and -27.3% (Supplementary Data file 2). Although the three glasses appear to have the same ablation bias, it is about 4% higher than that from zircon. Practical scan rates result in the superposition of multiple ablation spots and the scan should develop a V shaped profile since its central line receives many more pulses than the edges. The edge of each individual pulse has a relatively high brightness under BSE, concentrated at the edge of the scan where the pulse edges converge (Fig 4). As noted by Nasdala et al. (2006) for zircon, the brightness of BSE response increases with the degree of atomic disorder. This suggests deposition of Pb-depleted melt around the edge of the ablation footprint or the removal of melt that had previously formed within it. If the absolute plasma bias can be determined once using a solution, the offset between it and total measured bias should remain the same for a given set of laser operating conditions, providing a relatively easy way to routinely measure plasma bias.

https://doi.org/10.5194/egusphere-2026-2779
Preprint. Discussion started: 10 June 2026

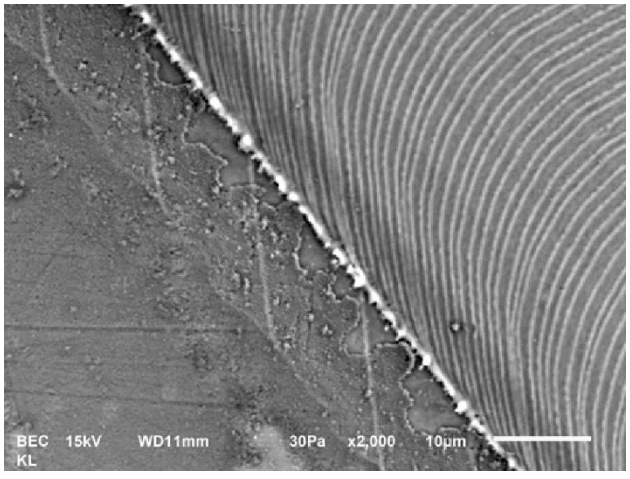

Figure 4: BSE high contrast image showing one side of a laser scan of KL. Bright fragments of melt are seen concentrated along the edge of the scan and ejected from it. These should be deleted in Pb relative to U contributing to a positive 206Pb/238U measurement bias.

3.2 Ablation bias

3.2.1 Understanding the ablation process

It has long been noted that during spot ablation of zircon, time resolved analytical (TWA) measurements of $^{206}Pb/^{238}U$ are found to increase especially for relatively narrow spots. The bias increases as a function of the aspect ratio of the pit with an early rapid rise changing to a slower linear rise, eventually levelling off and then dropping as emission becomes much weaker (Paton et al. 2010; Eggins et al. 1998). Downhole fractionation appears to be reduced with shorter laser wavelength and pulse duration, the femtosecond laser showing less fractionation than nanosecond lasers (Kimura et al. 2015).

Ablation bias still appears to be poorly understood. It depends on interaction of the sample with the laser, rather than plasma conditions, and is the most limiting for accuracy. Eggins et al. (1998) measured the fractionation of volatile Pb and Bi over refractory U and Th as a function of ablation pit depth in NIST612, as well as the geometry of the pit. They showed that Bi/Th increases with pit depth (downhole fractionation) until an aspect ratio (depth/surface diameter) of about 3:1 where the bottom of the pit had tapered to a diameter of about 1/3 of that at the surface and signal intensity was reduced by an order of magnitude. Subsequently, downhole fractionation reversed with Bi/Th decreasing. They concluded that the principal mechanism for elemental fractionation is condensation of the more refractory elements on the walls of the pit. In contrast, Kroslakova and

https://doi.org/10.5194/egusphere-2026-2779
Preprint. Discussion started: 10 June 2026

Günther (2007), after aerosol dilution experiments, concluded that elemental fractionation is at least partly a result of interaction of the ablated material with the plasma.

The ZrO_2-SiO_2 phase diagram determined by Butterman and Foster (1967) shows the appearance of a melt, consisting of ZrO_2 and liquid SiO_2, at about 2250ºC for the zircon composition with a single liquid above 2400ºC. As shown by Davis (2008), zircon decomposes to these two phases below 1500ºC in the presence of excess silica. Kosler et al. (2005) concluded that during ablation of zircon the retention of U in the dissociated ZrO_2 phase with release of volatile Pb is the reason for increasing Pb/U implying that fractionation in zircon is an effect of mineralogical changes in the target. However, this does not explain why minimal ablation bias is seen at the start of a $^{206}Pb/^{238}U$ time resolved analytical (TRA) profile for zircon.

It is instructive to carry out a rough calculation of the expected temperature increase of the target during ablation. This should be a function of the laser energy flux, expected absorption volume and specific heat of the mineral. A typical laser configuration delivers about 30 microjoules per pulse to a 30 micron diameter target. Assuming that the energy is absorbed in a 0.1 micron layer, roughly consistent with observed ablation rates, a target with a heat capacity typical of zircon (0.75 J/g-C), would be exposed to energy an order of magnitude greater than that required for melting (estimated temperature increase of about 10000ºC assuming constant specific heat). At this energy flux, it is likely that all minerals boil and produce a transient ablation cloud.

Melt should boil off during irradiation down to a depth at the base of the pit where temperature falls below the boiling point. Zircon ablation pits typically show a layer of solidified melt at the base and along the walls (Fig. 5), which could represent a Pb-depleted reservoir. To test this hypothesis, a wide (130 mic) pit was ablated into KL zircon. It was hoped to form a melt layer around the wall that was thick enough to sample (10 mic or greater). However, the wall layer proved to be only a few microns wide. Examination of the pit shows that the sides are smooth and somewhat wavy in shape whereas the bases are partly floored by an irregular layer of melt lying on top of a smooth surface (Fig 6A). The pit was sampled by passing a 30 micron beam across it. The scan shows an order of magnitude reduction in ^{238}U signal intensity within the pit, (Fig 6B) which is probably because of limited coupling of the laser to the highly uneven surface. There is also a decrease in $^{206}Pb/^{238}U$ ratio of up to 40% (Fig 6C, Supplementary Data File 3) with wall-adjacent material showing the lowest values in both emission and ratios. It is therefore clear that the basal melt is depleted in Pb and represents at least part of the reservoir that balanced the measured Pb-enriched material.

https://doi.org/10.5194/egusphere-2026-2779
Preprint. Discussion started: 10 June 2026

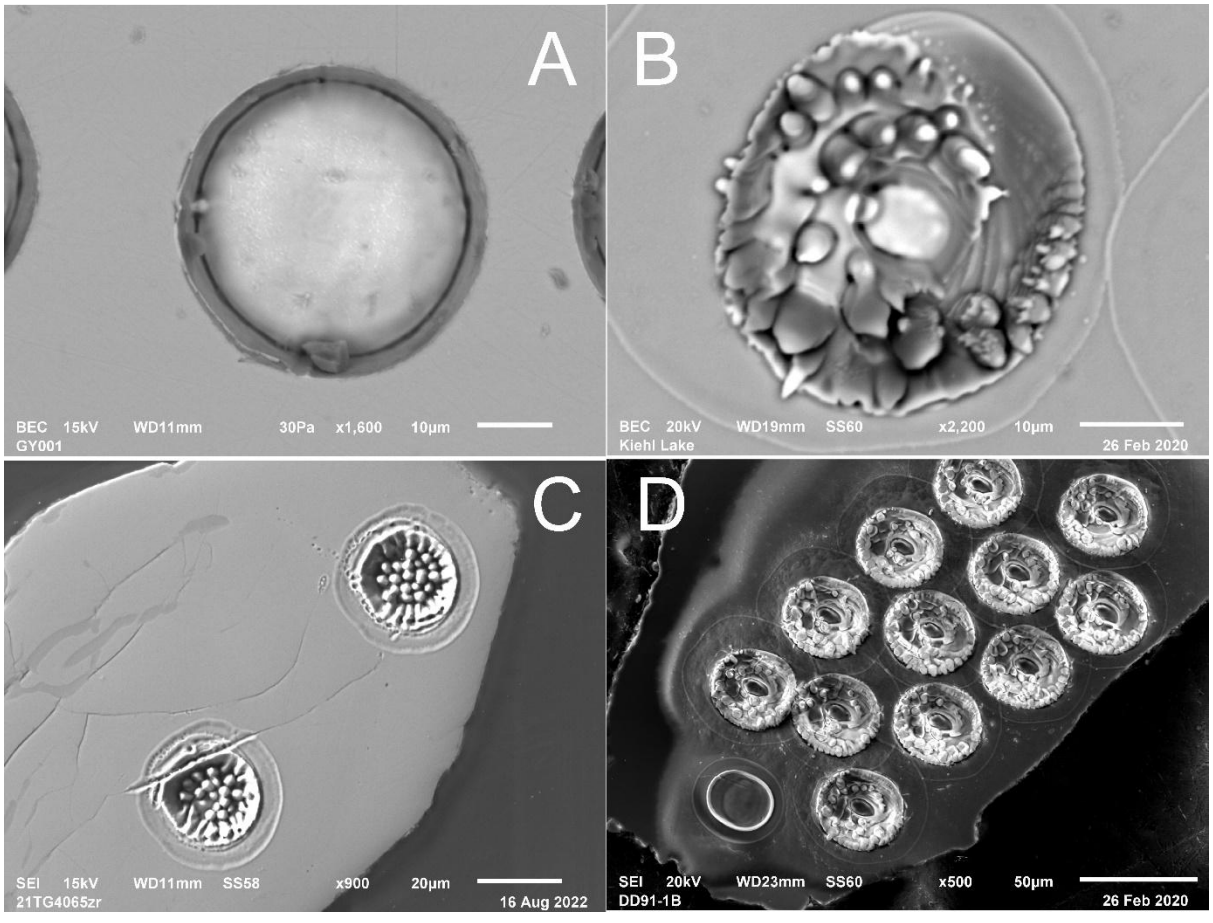

Fig. 5. (A) Electron backscatter image of laser ablation pit in KL zircon. (B) Same as A except that the laser beam was rotated once around a path half the radius of the pit. This shows that despite the flat surface seen at the base of the pit in A, the sample was melted. (C) Secondary electron image (SEI) of ablation pits in high-U Archean zircon that is much more damaged than KL. Irregular solidified melt is seen along the walls and base of the pits. (D) SEI showing ablation pits in DD91-1 produced by a rotating laser beam except for one nearest the lower left corner.

A potential approach to correcting ablation bias might be to measure the ratio of another pair of elements of different volatility, besides Pb and U, on the same grain. A possible candidate is Yb since it is the most volatile of the rare earth elements. HREE are enriched in zircon and are easily measured in most cases. If one could detect Yb/Yb* significantly higher than 1 (Yb* is the interpolated value of measurements of chondrite-normalized Tm

https://doi.org/10.5194/egusphere-2026-2779
Preprint. Discussion started: 10 June 2026

and Lu, the adjacent REE below and above Yb) and could demonstrate a proportional relationship with Pb/U bias, the latter could be corrected. Unfortunately, no significant Yb anomaly was detected in zircon within the percent resolution of our data (Fig 6D), indicating that Yb is insufficiently volatile compared to Pb.

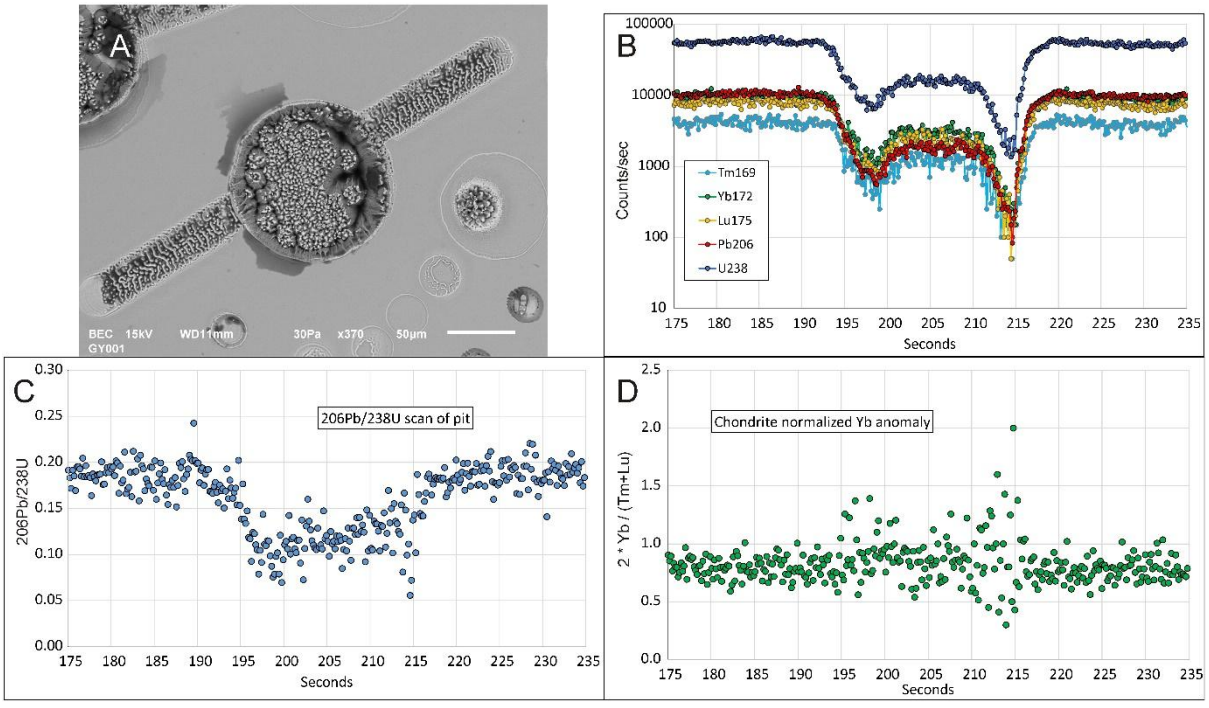

Fig. 6. (A) 130 micron pit floored by an irregular solidified melt layer crossed by a 30 micron scan line. (B) Trace element signals from the scan. (C) $^{206}Pb/^{238}U$ ratios show a depletion of Pb relative to U across the bottom of the pit. (D) 172Yb signal shows no clear anomaly relative to the average of less volatile 169Tm and 175Lu above and below it, indicating that Yb is insufficiently volatile to act as a proxy for Pb during ablation.

The usual way to correct for ablation bias is to measure a standard of similar composition (matrix-matched) under the same conditions as the sample, fit all or part of the $^{206}Pb/^{238}U$ time resolved analysis (TRA) profile for the standard to a curve, extrapolate it to zero time to determine the total bias correction, and apply this to the unknown using a similar extrapolation of its data (Paton et al., 2010; Gehrels et al., 2008). A complication with zircon is that, although most natural zircon is of similar composition, the crystal structure can be damaged by alpha recoil associated with the decay of isotopes in the U and Th decay series. In cases of old high-U zircon the

https://doi.org/10.5194/egusphere-2026-2779
Preprint. Discussion started: 10 June 2026

crystal structure can be reduced to a disordered (metamict) state, which should reduce the melting temperature, increase the amount of ablated material and modulate the profile. Zircon commonly shows oscillatory zoning of U, which can cause variability in damage and degree of melting by the laser. A mitigating factor is that highly damaged zircon is likely to be Precambrian in age where, because of the shape of the U-Pb concordia curve, ages determined from $^{207}Pb/^{206}Pb$ ratios are much more accurate and precise than those based on $^{206}Pb/^{238}U$ measurements. Isotope ratios from a single element are much less biased by ablation than those involving Pb and U so the TRA profiles for $^{207}Pb/^{206}Pb$ are usually constant over the course of an analysis. As the sample age becomes younger, $^{207}Pb/^{206}Pb$ age precision is increasingly degraded because of the shallow angle of the concordia curve relative to the Pb isotope ratio measurement line. For Phanerozoic ages the $^{206}Pb/^{238}U$ system must be relied on but younger zircon should generally have less damage, especially if samples are annealed before being ablated. Taking data from scan lines rather than spots is one approach to mitigating this problem but may also be affected by some degree of ablation bias (Fig. 1). In any case scans are not possible with most zircon, which consists of grains no more than a few hundred microns in size, which may have complex structures that need to be analyzed with spots.

The mechanism of progressive Pb/U fractionation must be understood for there to be any possibility of using complete data sets to accurately constrain the unbiased value of the $^{206}Pb/^{238}U$ ratio. Potentially useful information can be inferred about the ablation process from the cross-sections of actual pits documented by Eggins et al. (1998) using NIST612. The 300 pulse pit (Fig 6 in Eggins et al., 998) is most comparable in dimensions to a typical analytical pit in zircon. All pits are slightly flared at the mount surface with diameter decreasing as the base is approached. The walls of the pit are covered by a uniform thickness (about 5 microns) of brighter material, which consists of two thinner (about 0.2 of the total wall thickness) relatively bright sub-layers on the outside and inside, with a greyer layer in between. The inside exposed surface can be seen in Fig. 3b of Eggins et al. (1998) to consist of flow banded material, which could represent deposit or wall melt from the ablation plume. This layer seems somewhat discontinuous in cross-section and it may be a continuation of the middle grey layer. The thin outer layer has the highest and most consistent brightness. Both bright layers merge into a single convex-shaped layer over the base. The brightness of secondary electron images is usually a result of electrons being emitted from surfaces at high angle. This suggests that the thin bright layers enclose numerous surfaces left from fracturing or boiling.

The pit sections in Eggins et al. (1998) were exposed by ablating between two pieces of NIST610 glass fitted together along polished surfaces. It is therefore conceivable that the exposed wall features might have

https://doi.org/10.5194/egusphere-2026-2779
Preprint. Discussion started: 10 June 2026

resulted from penetration of the ablation cloud along the connecting surface but they seem much too regular to be explained this way.

Based on Fig. 2 of Eggins et al. (1998), the diameter of the laser beam is about equal to the opening of the pit. The sheath of glass observed at the edges of pits in zircon (Fig. 5, this work), approximately corresponds in thickness to the pit wall layers seen in Fig. 6 of Eggins et al. (1998). Their thickness remains constant with depth in pits over a wide range of aspect ratios.

The volume of the inner layers on the walls is roughly comparable to what might be expected from deposits left inside during excavation of the pit based on the assumption that deposit is proportional to wall area relative to the area of the pit opening as well as the observed drop in signal intensity. Wall area increases as the pit deepens, sequestering more deposit, but its thickness should not change rapidly and the fluted shape of the wall near the surface may have been eroded out by expansion of the ablation cloud.

Wall deposits should consist of material that is much less Pb-depleted than the base and may even be Pb-enriched, so they are not likely a component of the depleted reservoir. These deposits may be represented by the 2 inner layers while the outer bright layer represents the edges of the basal layer at previous depths, covered with semi-liquid deposit. The photos of cross sections in Eggins et al. (1998) also show the buildup of fallback deposit, which continues past aspect ratios well above those used for zircon analysis.

To summarize, three reservoirs are recognized as possible contributors to Pb/U signal fractionation: basal melt, wall deposit and fallback. Volatilization of melt at the base (bright outer layer in Fig. 6 of Eggins et al., 1998) is probably the main if not the only contributor to the signal and may be the only reservoir affected by recycling. Pb is considerably more volatile than U and significant evaporation should occur from boiling material at the base. Experiments collecting the ablated fraction show that it consists of solidified micro-droplets (Kosler et al., 2005), which would have an enormous surface area. Although their interiors should be Pb-depleted, they provide the main surface onto which Pb vapour is likely to condense and therefore should provide a Pb-enriched signal. The strong positive relationship between ablation bias and aspect ratio of the pit suggests that deposition of part of the ablation cloud either on the pit wall and/or as fallback plays a major role. Larger Pb-depleted melt droplets should be preferentially deposited as fallback and possibly as pit wall deposit, enhancing fractionation of the signal.

3.2.3 Measuring ablation bias

^{238}U could be used to represent the ablation signal if its concentration were uniform. However, U is typically zoned in zircon. Hf was also found to be zoned, following a similar pattern to U. Therefore, a Zr or Si

https://doi.org/10.5194/egusphere-2026-2779
Preprint. Discussion started: 10 June 2026

oxide species must be used. Si-oxides have a high background due to the use of a silica plasma torch but $^{90}Zr^{16}O$ typically produces a signal $^{106}(ZrO^{+})$ comparable to that from ^{238}U and is therefore ideal. The suggestion that the $^{206}Pb/^{238}U$ profile is controlled by increasing sequestration of depleted material is supported by the fact that the ZrO signal loss (1 minus the signal normalized to an assumed zero-loss value), has a similar (inverted) shape to the $^{206}Pb/^{238}U$ profile at least for undamaged zircon. This is illustrated below with data on zircon grains from samples KL and DD91-1.

To acquire useful data from the earliest pulses, measurements were carried out in which single laser pulses were fired at the sample spot each 5 sec (0.2 Hz) and the signals continuously measured on ^{106}ZrO (10 msec), ^{206}Pb (20 msec) and ^{238}U (10 msec). A similar approach was suggested by Cottle et al. (2009) for routine dating of zircon. To assure stable emission, the laser was left running at 10 Hz with the beam blocked, and a 5 sec warm-up time assigned between single pulses. One spot was programmed with 300 passes, which required 1500 sec to fully analyze. Software to remove baseline noise and integrate each pulse is given in Supplementary Data File 4 along with results. The pulse profiles were averaged to give the instrument response functions for each mass signal, which are found to be indistinguishable after normalization (Fig. 7). If Pb continuously evaporated from a melt phase within the pit, the average ^{206}Pb curve should appear broader than the others, which is not the case. Similar measurements were carried out at 10 Hz on the same samples and gave similar $^{206}Pb/^{238}U$ profiles after signal stabilization.

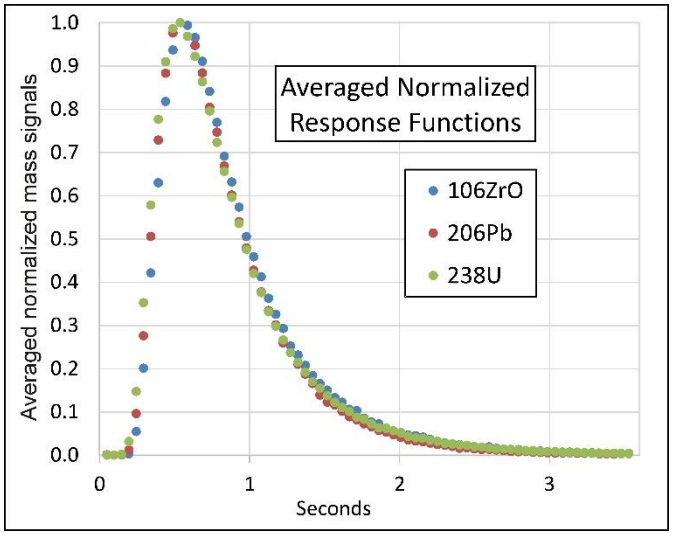

Fig 7. Averaged progressive single shot signal responses normalized to highest values for masses from KL.

https://doi.org/10.5194/egusphere-2026-2779
Preprint. Discussion started: 10 June 2026

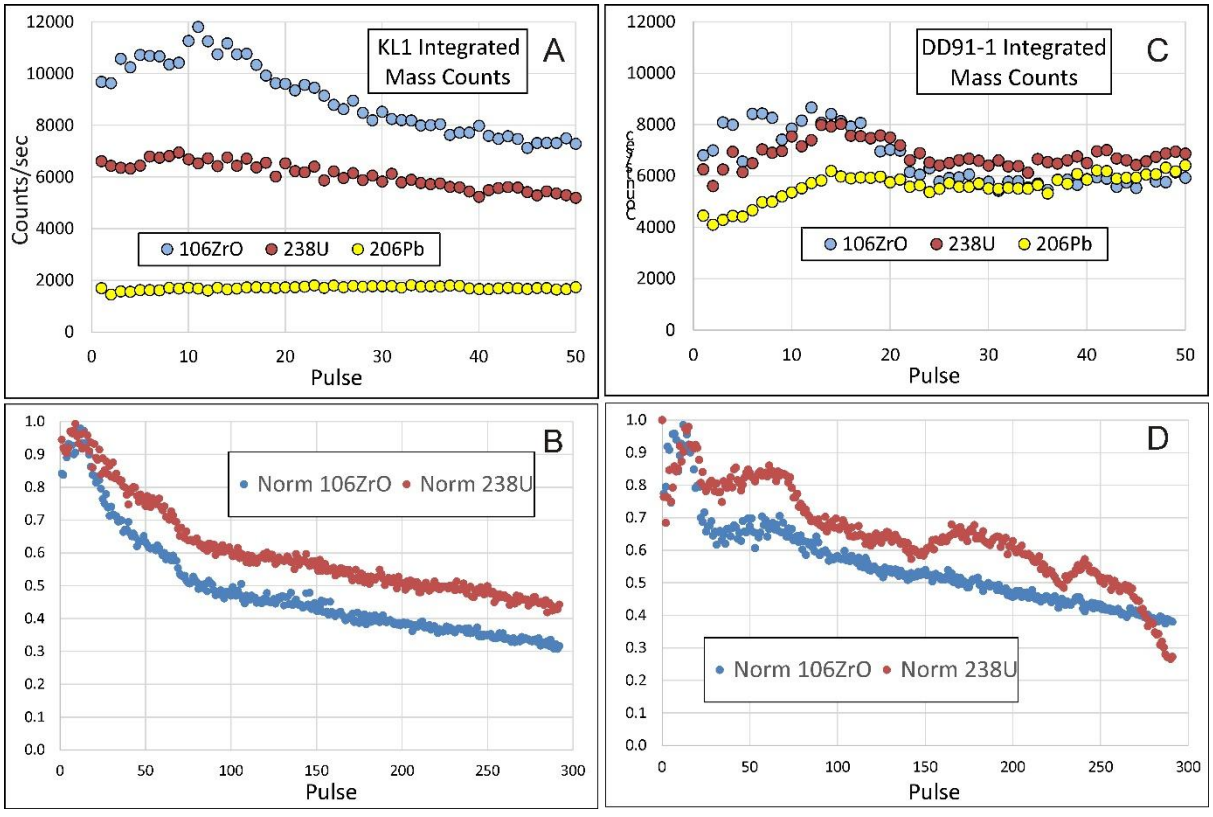

Fig 8: Signal profiles for 0.2 Hz analysis on standards KL (A, B) and DD91-1 (C, D). (A and C) signals in counts per second for the early parts of the analyses showing relatively constant or slightly increasing intensity for the first 11 pulses. (B and D) signals normalized to values at the 11th pulse (highest ^{106}ZrO),

Analytical profiles for ^{106}ZrO and ^{238}U from KL and DD91-1 are shown in Fig 8A-B and Fig 8C-D, respectively. Data are presented in Supplementary Data File 4. The assumed zero-loss signal intensities used for normalization of ZrO and U are taken as the maximum recorded signals (Fig. 8A and 8C). For both samples the ZrO intensity is found to increase to a maximum at around 10 pulses and then decrease. It is common with data taken at 10 Hz to see a rapid signal rise over the first half-second followed by a more gradual rise that peaks over 1 to 2 seconds and then begins to decrease as with the 0.2 Hz data. The 0.2 Hz data show that this peak is not just a property of the transfer function but of the actual signal. This suggests that fallback is a major source of signal loss for the earliest pulses when the pit is shallow and ablation cloud expansion has a large lateral component. Successively larger proportions of ablated material should remain in the deepening pit, while the fraction of material

https://doi.org/10.5194/egusphere-2026-2779
Preprint. Discussion started: 10 June 2026

contributing to fallback might be expected to decrease as the pit deepens and the ablation cloud is directed more strongly upward. Since the pit always has an opening equal to the beam diameter, some material will always escape. Therefore, the pit must continuously deepen and, with successive pulses, an increasing proportion of the ablated material should be deposited on the walls. This requires that the base of the pit become progressively narrower as confirmed by Eggins et al. (1998).

The main difference between the signal profiles for KL and DD91-1 is that U zoning in DD91-1 creates fluctuations relative to the ZrO curve (Fig. 8B vs. Fig 8D). The ZrO curve from DD91-1 also shows an increase between pulse numbers 30 and 70. This corresponds to an increase in U concentration so it might reflect higher radiation damage leading to evaporation of more sample by each pulse. The measured $^{206}Pb/^{238}U$ profiles, normalized to the known primary ratios biased by an estimate of plasma-induced fractionation (see below), are presented for the KL and DD91-1 samples in Fig 9 where they are compared to curves that represent the relative proportion of material deposited within the ablation cell. These curves are determined as 1 minus the normalized ZrO signals (1 – NZi) for each pulse i. The normalization factors are set at the maximum count rates, which is the minimum value possible and provide a good fit with the early parts of the ratio profiles. A higher number would uniformly elevate the curves, which are somewhat similar in shape to the measured ratio profiles but rise faster. Multiplying the normalized ZrO depletion curve for KL by a factor of 0.78 results in a good fit over most of the measured profile, while a factor of 0.90 optimizes the fit for the DD91-1 curve, which shows local complexities. These factors should represent the fraction of Pb lost from the deposits, assuming that there is no recycling. Both curves are inconsistent with the inference that emission is proportional to the exposed area of the base, which should result in a linear loss of primary signal to about half for a 20% reduction in base diameter (aspect ratio of 0.8). This would require progressively decreasing the normalization factor which would result in lowering the rate of deposition, causing the latter half of the curves to turn over and begin decreasing, as shown on Fig 9. Eggins et al. (1998) noted that the excavation rate of pits increased with pit depth, presumably because of increased reflection of laser energy off the pit walls. However, their measured rate of increase was not sufficient to maintain the same ablation volume with each pulse. It may be that in this case there is some recycling of deposit near the edge of the pit.

https://doi.org/10.5194/egusphere-2026-2779
Preprint. Discussion started: 10 June 2026

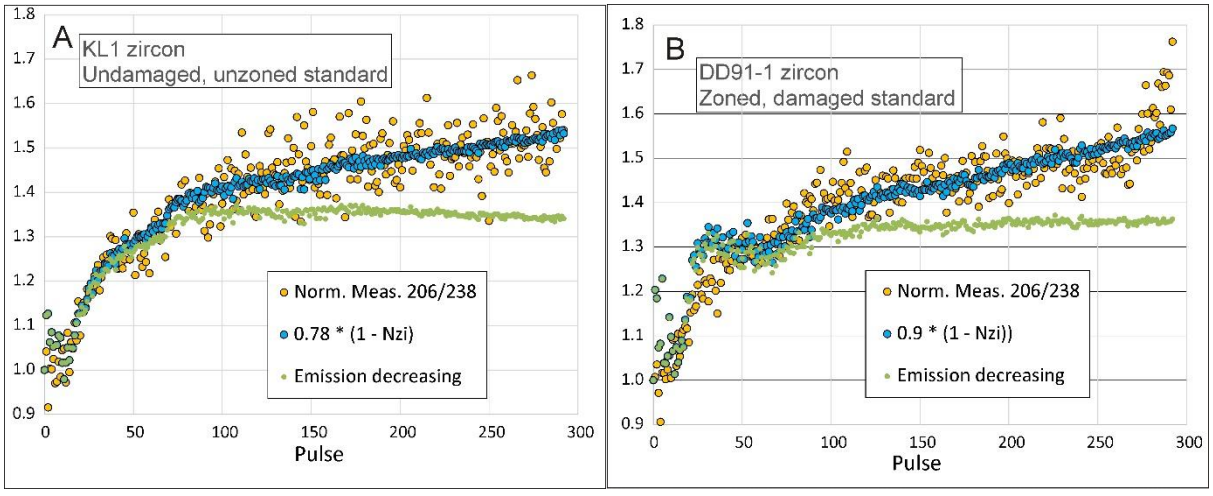

Fig 9: Signal profiles for 0.2 Hz analysis on standards KL (A) and DD91-1 (B). 206Pb/238U profiles (orange circles) normalized to estimates of plasma-biased true values compared to profiles of ablation deposits scaled by Pb depletion values chosen to maximize fit to ratio profiles (blue circles). Green dots are the same profiles assuming that ablated mass is proportional to area of the base of the pit with a final aspect ratio of 0.8

3.2.4 Consistency of early ratios

There is a notable mismatch to the main fractionation profile over the first 10 pulses from both samples where the ratio measurements show no consistent increase (Fig. 10). For KL, the average of the first 10 absolute $^{206}Pb/^{238}U$ measurements is 0.1231 ± 0.0038, which corresponds to a plasma bias of -31.5%. while for DD91-1 it is 0.3549 ± 0.0091, corresponding to a plasma bias is -31.2%, showing that results in this case are consistent. The first 10 pulses correspond to an anomalous period of increasing emission, which might be explained by rapidly decreasing fallback, but this does not explain the quasi-constant ratios. Melting and partial volatilization of basal material should produce maximum signal ablation bias with the earliest pulses, decreasing to an unfractionated value as an equilibrium is established between production and consumption of the basal Pb-depleted reservoir (e.g. Fig. 6C). Once melt depletion in Pb compensates vapour enrichment, the composition remains constant. The early downward fractionation trend should be opposed by deposition of fallback forcing signal fractionation upward. Eventually, fractionation from the target material reaches its equilibrium value of zero and the ratio trend becomes dominated by deposition of Pb-depleted material. Boiling of a relatively deep melt pool resulting in ejection of larger melt droplets might account for the rapid increase in ratios, which is usually seen during the

https://doi.org/10.5194/egusphere-2026-2779
Preprint. Discussion started: 10 June 2026

early part of the profile. As a larger proportion of deposit becomes confined in the pit, deposition of fallback may linearly increase producing similar growth of the fractionation profiles, as is typically seen in measured results.

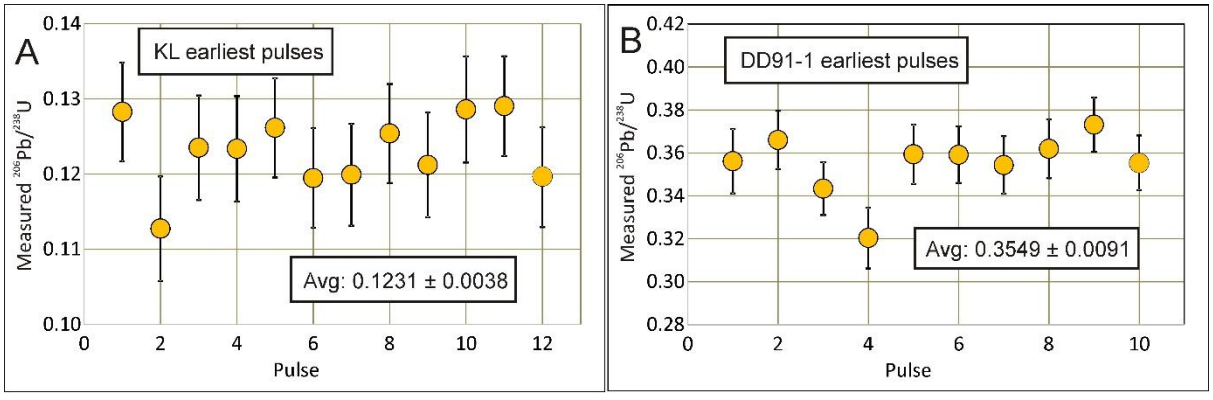

Fig 10: Averages of earliest ratios from KL (A) and DD91-1 (B). Errors represent 2 sigma.

Without an understanding of fractionation processes, it might be assumed that the earliest pulses are of greatest importance for constraining the ablation bias-free age. To evaluate this, experiments were conducted on KL, DD91-1 and a relatively low-U but zoned Archean standard, DD85-17, using laser frequencies of 0.2 Hz and 10 Hz, where results from the first 5 pulses must be omitted. Data sets shown in Figs 11A and B were acquired during different sessions so plasma bias (Y-intercept) cannot be compared between them. The number of pulses analyzed was between 50 and 60.

Data in Fig 11 are averages of 4 to 6 runs for each sample. Data from individual runs are shown in Supplementary Data Files 5 and 6 for runs carried out at 0.2 Hz and 10 Hz, respectively. Although the average ratios show a linear increase, about half the individual 0.2 Hz runs show $^{206}Pb/^{238}U$ ratios in the first ten pulses that do not obviously increase or increase more slowly than ratios from subsequent pulses. The Y-axis intercept of the average regression line from DD91-1 is distinctly (~5%) higher than intercepts from the average KL and DD85-17 data (Figs 7A and B). One might expect a higher slope from a more damaged zircon such as DD91-1. KL should be the least damaged because of its relative age and U concentration but DD85-17 shows the lowest intercept and slope. The variability of intercepts within a single session suggests that apparent ablation bias from the earliest pulses can be chaotic and can be affected by radiation damage. Therefore, this approach cannot be used to determine plasma bias or remove biases by comparing to a zircon standard.

https://doi.org/10.5194/egusphere-2026-2779
Preprint. Discussion started: 10 June 2026

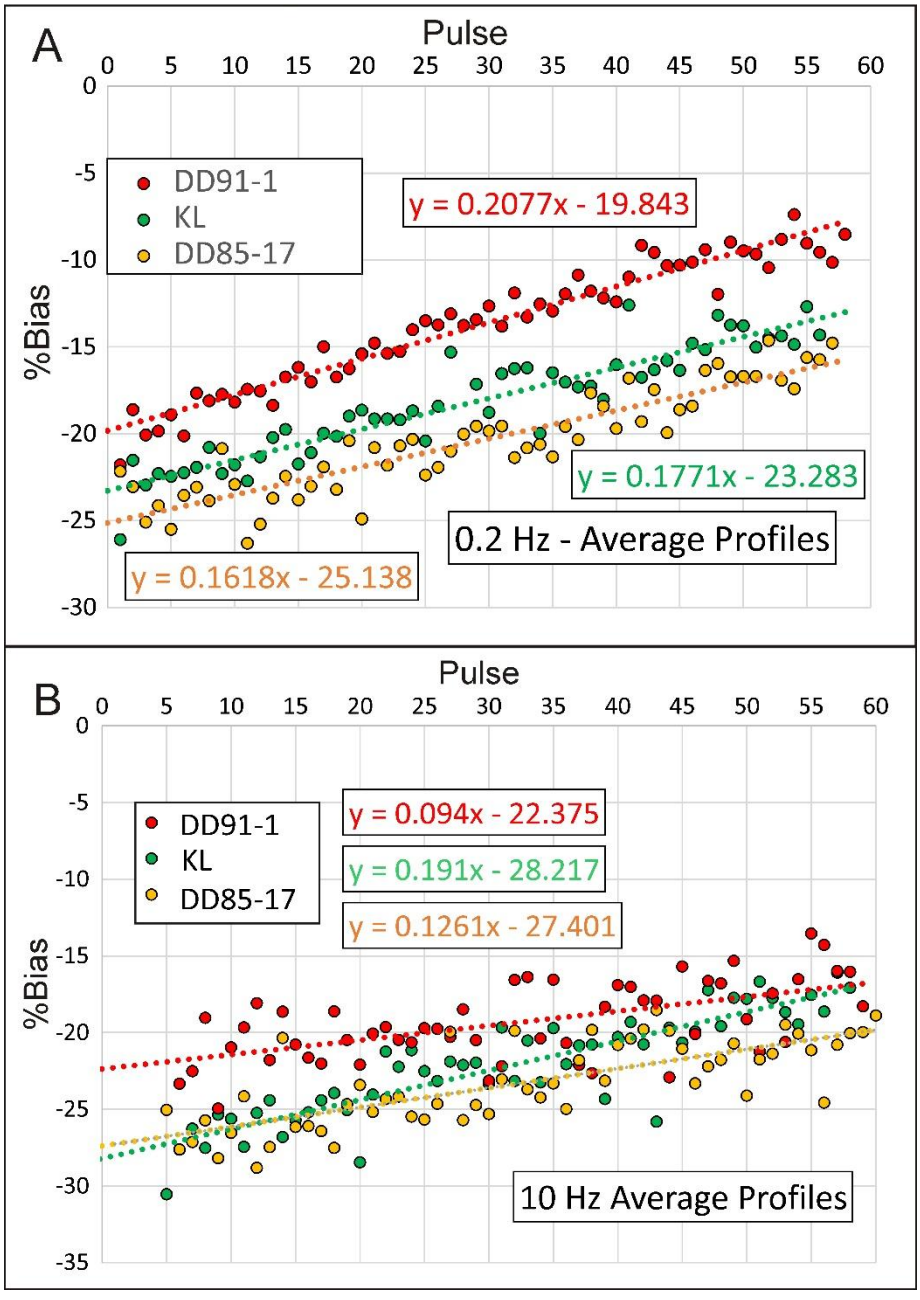

Fig. 11 Percent difference between the measured and true $^{206}Pb/^{238}U$ ratios of three zircon standards for data acquired at (A) 0.2 Hz and (B) 10 Hz. Each set of symbols represents an average of analyses on 4 spots. Analyses shown in A and B were carried out during different sessions with different plasma bias.

https://doi.org/10.5194/egusphere-2026-2779
Preprint. Discussion started: 10 June 2026

3.2.5 Modelling ablation

The above data show that in general if not always in detail there appears to be a consistent relationship between the observed $^{206}Pb/^{238}U$ profiles and signal decay curves for zircon. This suggests the possibility of modelling $^{206}Pb/^{238}U$ bias. A simple conceptual sketch of the excavation process that might underpin such a model is shown in Fig 12A. The first laser pulse leaves a shallow (~0.1 mic) pit with a Pb-depleted layer on the base and a small amount of possibly Pb-enriched material along the rim wall as well as fallback material deposited outside the pit, which cannot be recycled. In Fig 12A the second laser pulse ablates much of the depleted material in the base of the pit while material previously deposited on the walls absorbs energy from the beam while being re-ablated, which results in the diameter of the flat base decreasing with depth. This exact process is unrealistic since it results in a pit that narrows much too fast, with the base disappearing at an aspect ratio (depth/diameter) of about 0.2 but it suggests that narrowing of the pit can be an effect of sculpting the target material rather than just the buildup of deposit.

As shown schematically in Fig 12B, successive laser pulses will form clouds of ablated target material, some of which may include a proportion of previously fractionated deposits, which would impose a Pb-depleted fractionation on the cloud. Formation of new deposit from the cloud will impose a net Pb-enrichment, which is what is measured. The only difference between fallback and pit deposits is that fallback cannot be recycled. Most pit deposit is also probably not recycled because of the steep angle of its surface relative to the laser beam. The relative amount of material deposited on the wall and as fallback, possibly modified by variable Pb/U fractionation and degrees of re-ablation of previous deposits, should be proportional to the difference between the measured signal attenuation curve and what the signal would be if there was no deposition, assuming that equal amounts of material are ablated by each pulse.

https://doi.org/10.5194/egusphere-2026-2779
Preprint. Discussion started: 10 June 2026

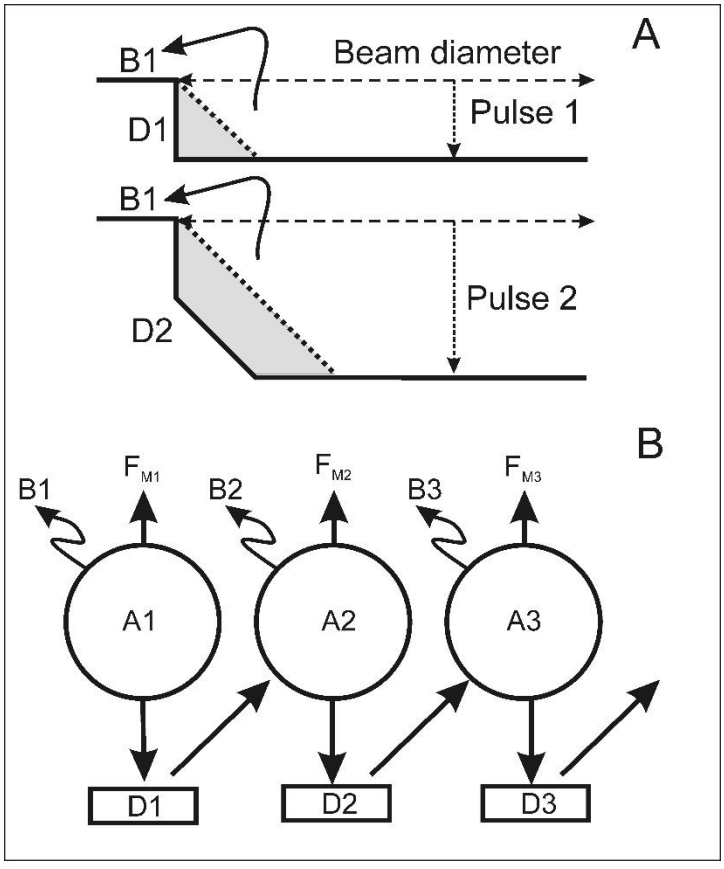

Fig 12 (A) Schematic illustration of the model showing the effect of the first two laser pulses on a zircon sample as seen from the edge of a cross section of an ablation pit. D is the depth excavated per laser pulse. Pb-depleted ablated material (melt) deposited in the pit is shown in grey. The second pulse is assumed to re-ablate the residue left from the first but this consumes energy at the edge of the beam, causing the pit to taper with depth. (B) Effects of the first laser pulses on measured composition. The first ablation cloud (A1) leaves a Pb-depleted deposit in the pit (D1) and fallback (B1), which increase its Pb/U ratio. The second pulse can re-evaporate D1 plus pristine material, leaving a second Pb-depleted deposit (D2) as well as fallback (B2). Absorption of Pb-depleted D1 will reduce the Pb enrichment effect on the composition of the cloud that deposits D2. Fallback should produce an increment of Pb-enrichment.

The mathematical expression of a general model for progressive fractionation of $^{206}Pb/^{238}U$ from zircon using the observed signal decay as a proxy for sequestration of fractionated deposit is developed in Appendix 1

https://doi.org/10.5194/egusphere-2026-2779
Preprint. Discussion started: 10 June 2026

and formulated in Excel in Supplementary Data File 4 as a series of recursive equations. These calculate the Pb fractionation of an ablation cloud after absorbing a previously fractionated target, and the measured value after sequestration of material as pit deposit and fallback. The Pb loss factor Li per pulse is 0 if there is no Pb loss and 1 if Pb loss is total. The proportion of recycling per laser pulse, Ci, in the equations can vary from no (0) to complete (1) recycling where each successive pulse completely abates the previous deposit. Recycling can only occur within the pit and may be limited by mixing with a melt reservoir at the base of the pit. Pb/U ratios from the first ten pulses, during which Pb-depletion in the basal melt approaches an equilibrium value such that the vapour is unfractionated, as discussed above, are simulated by decreasing the recycling factor progressively from 0.9 to 0, which removes the downward trend in modelled ratios.

All models start at 1 at pulse zero, which represents a theoretical value of $^{206}Pb/^{238}U$ divided by the ablation bias-free ratio. The measured ratios must be normalized to an estimate of the plasma-biased value of $^{206}Pb/^{238}U$ and the estimate adjusted to optimize the fit between the model and normalized measured profiles (Fig 13).

As expected from the match between deposit retention and ratio profiles, the model for KL data in Fig 12 can be made to fit the normalized ratio profile quite well with a loss factor of 0.78 and zero recycling while the best fit for DD91-1 data in Fig. 13 requires a loss factor of 0.90 with zero recycling. The model for this sample shows an anomaly between pulses 25-50 where both ZrO and U signals begin to increase, but this is not reflected in the measured ratio profile. The increase in ZrO emission suggests that this zircon zone is more damaged resulting in the pulses ablating more material. This would effectively raise the normalization factor which, if included in the calculations, would reduce or nullify change in the trend of the ratios. ZrO and U profiles from both samples show a discontinuity in slope at about 60 pulses, following a short (40-60 pulse) period of stasis. This corresponds to the beginning of a short rapid increase in measured ratios, which subsequently slows to form an extended linear trend. The rapid increase in $^{206}Pb/^{238}U$ at the end of the measured profile cannot be explained by the model. This is associated with a drop in U concentration but no change in the ZrO trend. The best explanation may be beam intersection with a significantly older core. Even though cores have never previously been noted in this sample, it is from an intrusion in metasedimentary rock which contains abundant older detrital zircon (Davis et al., 2002) .

https://doi.org/10.5194/egusphere-2026-2779
Preprint. Discussion started: 10 June 2026

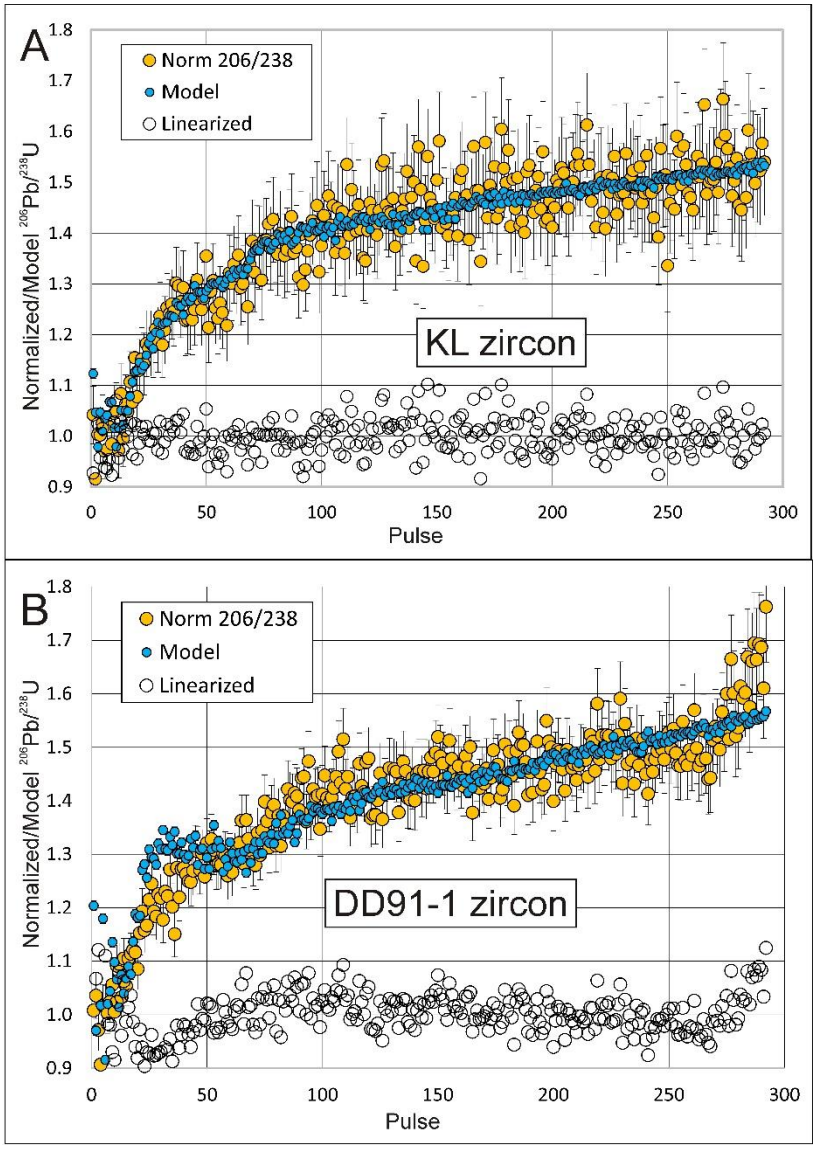

Fig 13: Normalized measured $^{206}Pb/^{238}U$ ratio profiles and modelling results from 0.2 Hz analyses of zircon KL-1 (A) and DD91-1 (B). Normalization factors, were taken from the mean of the first 10-12 data shown Fig 8. Pb loss is taken as constant at 0.78 for (A) and 0.9 for (B). Recycling is zero except for the first 10 pulses as explained in the text. Linearized data are explained in the text. Error bars represent 1 sigma estimates based on counts.

https://doi.org/10.5194/egusphere-2026-2779
Preprint. Discussion started: 10 June 2026

The aim of fitting data to a curve, whether empirical in conventional calibration or model-dependent, is to remove biases on all data, allowing them to be averaged to determine a more precise value for the $^{206}Pb/^{238}U$ ratio. Since all models start at 1, it is necessary to normalize each measurement in the ratio profile by a factor, R_0, that provides the closest match (minimum MSWD) between data and model. R_0 should then be the $^{206}Pb/^{238}U$ ratio corrected for ablation bias (although still affected by plasma bias). An error on R_0 could be determined from all the data by dividing the measured ratio values by the corresponding model value as shown by the 'linearized' points in Supplementary Data File 4. A realistic model should result in a randomly scattered distribution of adjusted measured data that fits a horizontal line. The weighted mean of this distribution should then give the best estimate of unbiased $^{206}Pb/^{238}U$ ratio and error based on all data. Unfortunately, this approach is not practical because there are too many degrees of freedom. In addition to uncertainty about the choice of a normalizing factor for the ZrO signal, fitting a model to the data also requires choosing Li and Ci factors. For example, a theoretical ablation model could be forced to exactly match data points by adjusting Li, and Ci for each laser pulse using an arbitrary Ro value but this would be meaningless. Similarly, adjusting one or two constant model parameters can produce acceptable fits with variable estimates of the unbiased ratio so this is also meaningless without independent knowledge of the parameters. Despite the apparent effectiveness of modelling in this case, it cannot by itself provide accurate correction of ablation bias. However, it provides a mathematical platform for testing ideas against observed data so might help improve understanding of the ablation process.

3.2.6 Correcting Pb/U bias

The Y-intercept of data from the early (rapidly increasing) phase of a ratio profile appears to be affected by the structural state of the zircon and so does not appear to provide a well-constrained estimate of plasma bias. It is notable that both ratio profiles show a linear increase from about 100 to at least 250 pulses corresponding to a linear decrease in ZrO signal. Gehrels et al. (2008) proposed regressing this section and using the Y-intersection of the standard relative to a sample to correct for bias. Both should be affected by the same bias so their ratio should be the ratio of the unbiased ratios. In this case, the ratio calculated from the intercepts is +0.9% (higher) than the true ratio, which is accurate within measurement errors.

A more conservative estimate might be based on averaging all, or most of, the $^{206}Pb/^{238}U$ profile. Despite profiles for both standards not being identical, the ratio of average profile ratios is only +0.20% different from the true ratio when the profiles are terminated at 260 pulses before the anomalous increase for DD91-1.

The most comprehensive way to compare sample and standard data would be to match a standard fractionation curve to that of a sample by varying a calibration factor affecting the standard $^{206}Pb/^{238}U$ ratios to

https://doi.org/10.5194/egusphere-2026-2779
Preprint. Discussion started: 10 June 2026

achieve a minimum MSWD. This approach is shown on Fig. 14. All the calculations are shown in Supplementary Data File 4 (KL Data sheet). Since this requires direct comparison between the two fractionation profiles, it reveals whether or to what extent standard and sample are an appropriate match. The normalized profile for DD91-1 is a remarkably close visual match for that of KL before the rapid increase in ratios in the last 30 pulses of the DD91-1 profile. Omitting this part, gives a calculated ratio 0.8437, which is +0.15% different from the true ratio. Given the differences between the normalized ZrO profiles found for KL and DD91-1 (Fig. 8), it seems surprising that the shapes of the measured ratio profiles for both zircon samples fit so well (Fig 14), which suggests that we still do not have a complete picture of the ablation process.

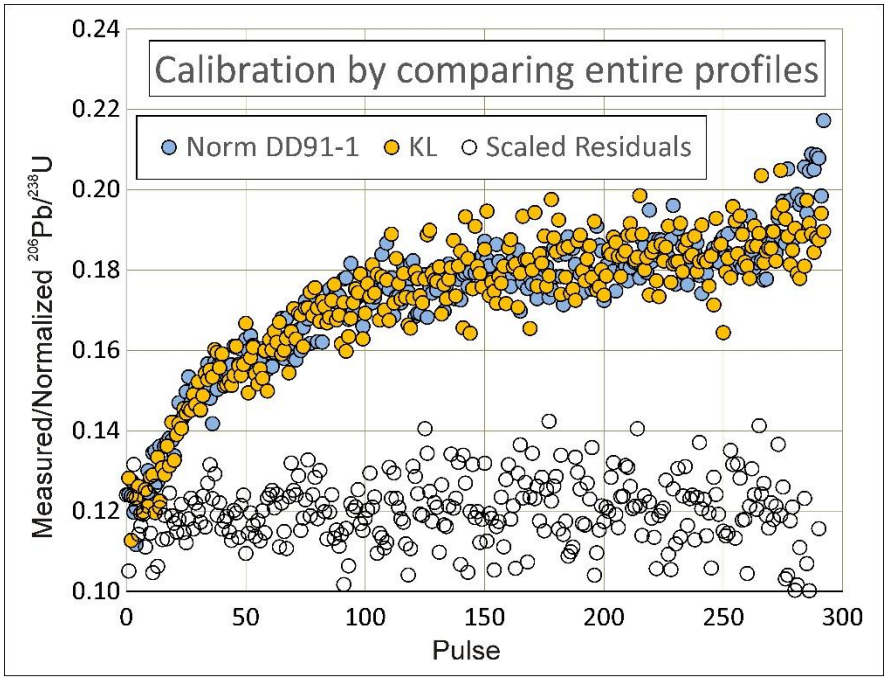

Fig 14: Comparison of measured KL ratio profile (taken as the standard) with measured DD91-1 profile (taken as the unknown) normalized to minimize the sum of squares of differences between corresponding data points (residuals). These are scaled so they are visible on the plot. The residual for two overlapping data would plot on the 0.12 line. Omitting the last 30 data, a normalization factor of 2.868 gives the minimum sum of residuals. The inferred 206Pb/238U value is 0.15% different from the accepted ratio.

https://doi.org/10.5194/egusphere-2026-2779
Preprint. Discussion started: 10 June 2026

A program has been written to easily process U-Pb data according to the above method of matching $^{206}Pb/^{238}U$ profiles between sample and standard. Data are entered into an Excel spreadsheet and processed using Visual Basic for Applications (VBA). The program, called UTILAZ (University of Toronto Isotopes Laser Ablation of Zircon) along with instructions, is given in Supplementary Data File 7. The average $^{206}Pb/^{238}U$ profile from standard measurements before and after a sample measurement is adjusted by a calibration factor calculated so that the sum of squares of the differences between sample and standard data is minimized between chosen limits of the profile. The approach proposed by Paton et al. (2010) and used in Iolite is similar except that it involves smoothing profiles using cubic splines. Matching sample and normalized standard profiles gives results that are very similar, but not identical, to just dividing the averages of the two profiles., but the comparison approach provides a better way to calculate errors from dispersion of the data as the square root of the mean of squares of differences between data divided by the number of data.

The program allows editing of data and is applied to Precambrian zircon. KL is chosen as the standard and, as mentioned, should be the least damaged, while JG-diorite, DD85-17 and DD91-1 are Archean with DD91-1 having significantly higher U. Sample 21CB-1242 has the highest U concentration and appears to be completely metamict. Alteration is clearly visible in BSE images and was avoided at the surface. ^{88}Sr was measured as a proxy for alteration at depth.

Results are shown in Table 1 (Supplementary Data File 8) and Fig. 15. The shapes of profiles for non-metamict samples generally match well with their adjusted standard profiles. Although their calibrated $^{206}Pb/^{238}U$ data scatter somewhat outside of errors, the averages are all within ±1% even though these grains should have been affected by a range of radiation damage. $^{206}Pb/^{238}U$ profiles from the metamict zircon are somewhat flatter than those from the standard and the calibrated data show reverse discordance from -6% to -19%.

Metamict zircon might be expected to ablate more rapidly, resulting in a deeper pit and more fractionation than the relatively undamaged standard. This should result in a larger and more rapidly decaying ZrO signal, which is generally the case (Supplementary Data File 7). The UTILAZ program includes the ability to adjust calibration factors according to ZrO signal profiles, which were fitted to exponential functions to calculate normalized decay signal profiles as in the previous models. Adjusting the standard calibration results in an over-correction for the data from the metamict zircon and makes the non-metamict zircon data more discordant. These results are not shown but can be replicated using the software. The average ZrO signals from all measurements are roughly constant (Supplementary Data File 7). They show no correlation with U concentration and damage, which seems surprising if metamictization results in greater ablation volumes. Higher fallback could be an explanation, but this is contradicted by the fact that data from the metamict zircon show a correlation between

https://doi.org/10.5194/egusphere-2026-2779
Preprint. Discussion started: 10 June 2026

reverse discordance and U concentration (Fig 15B). This might serve as a first-order correction to $^{206}Pb/^{238}U$ bias even though its cause remains unclear.

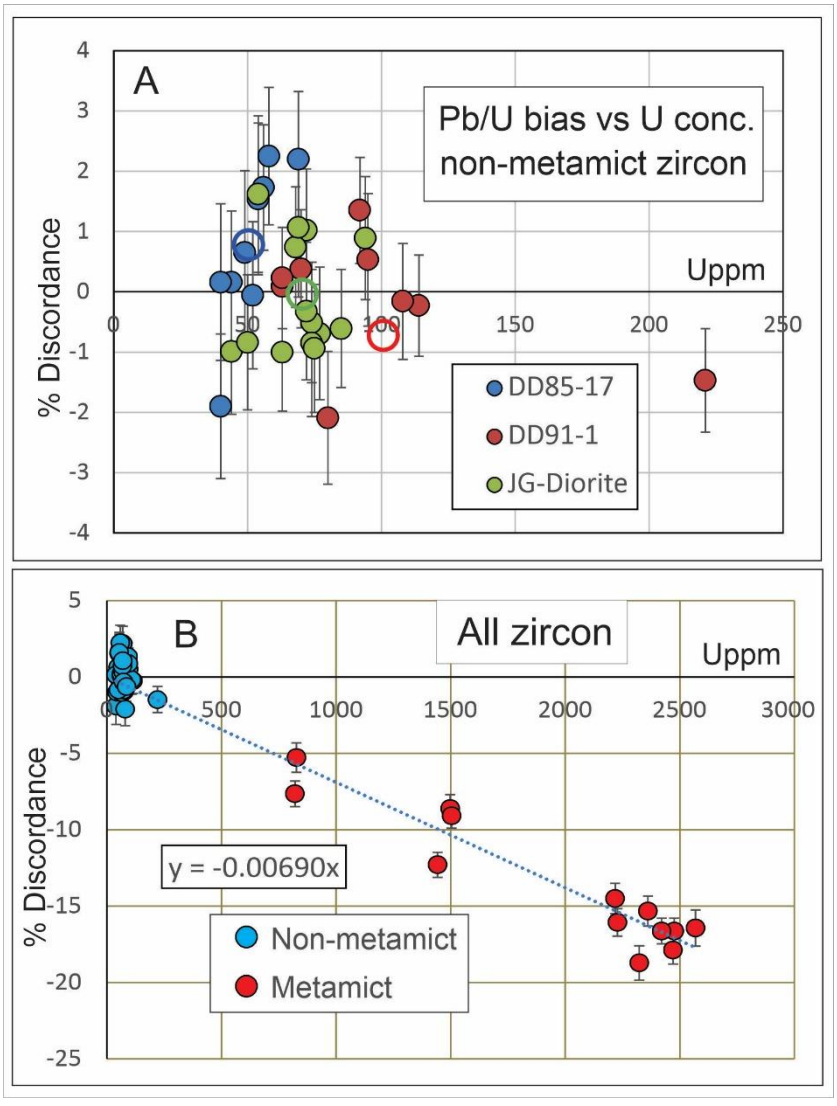

Fig 15: Results of UTILAZ data reduction on zircon with variable ages, U concentrations and radiation damage. Error bars represent 2 sigma. KL was used as the standard. (A) Data from non-metamict zircon. Open symbols represent averages. (B) Data from metamict zircon U (>500 ppm) show a roughly linear relationship between U concentration and negative discordance. The regression line is forced through the origin.

https://doi.org/10.5194/egusphere-2026-2779
Preprint. Discussion started: 10 June 2026

A final remark concerns the contrast in ablation response of monazite. $^{206}Pb/^{238}U$ profiles for monazite tend to be flatter than those for zircon and in cases of narrow (<15 mic) beams may appear flat. Examination of pits in monazite reveals much less evidence of melted deposit if any. This is most likely because ablation is accompanied by the production of the gas phase P_2O_5, making it more explosive. Unfortunately, further work showed that ablation profiles, while flatter than with zircon, are less consistent. Ablation of carbonates and phosphates should also produce gas phases. Since they are often used for dating, further study should be useful to understand and help correct their biases.

4. Conclusions

Measurement biases on $^{206}Pb/^{238}U$ in LA-ICPMS can be divided into plasma-induced and ablation-induced. Line scans of NIST glass standards are affected by higher ablation bias than scans on a megacrystic zircon standard such as Keuhl Lake (91500). Determining plasma bias by measuring proxy elements should be theoretically possible but requires understanding how the mass discrimination factor depends on mass.

Down-hole fractionation of measured $^{206}Pb/^{238}U$ during laser ablation of minerals is a result of the release of volatile Pb during boiling of the ablated sample followed by sequestration of Pb-depleted melt droplets as fallback around the pit and along pit walls. Pb/U fractionation during the first 10 or so laser pluses is the result of approach to isotopic equilibrium between Pb-depleted melt and Pb-enriched vapour, opposed by deposition of Pb-depleted material. These might produce apparently constant ratios but the results are chaotic and the measured ratios will always be biased toward high Pb/U. Subsequently, the effect of Pb-depleted fallback dominates, leading to a rapid rise in measured $^{206}Pb/^{238}U$ ratios. This is followed by a slower rate of increase after about 80 pulses as sequestration along the wall of the pit becomes dominant and finally a linear increase in ratios that corresponds to a linear decrease in signal strength. The measured profile can be broadly modelled using the ^{106}ZrO and ^{238}U signal profiles as a proxy for the amount of sequestered material and the effect of U zoning. Models suggest a high degree of removal of Pb from the ablation cloud and a low degree of re-ablation (recycling) of sequestered material. However, modelling cannot accurately constrain the unbiased ratio (age) because of unconstrained variations in these two parameters. Extrapolation of early data profiles (first 60 pulses) appears to be ineffective for constraining the ablation bias-free $^{206}Pb/^{238}U$ value. They give plasma bias values that do not agree for different zircon samples and that may be influenced by crystal damage.

A variety of approaches for calibrating Pb/U ages using standards include comparing average $^{206}Pb/^{238}U$ values, Y-intercepts of linear sections of profiles (Gehrels et al. 2008) or preferably, normalizing the sample

https://doi.org/10.5194/egusphere-2026-2779
Preprint. Discussion started: 10 June 2026

profile until it matches the standard profile as closely as possible. Software is provided for data reduction based on this approach, which seems effective provided samples are not metamict.

The easiest approach to determine the plasma bias during a session is with laser line scans of megacrystic zircon standards or NIST glasses. The offset in $^{206}Pb/^{238}U$ due to ablation bias during the scan under the same ablation conditions would need to have been empirically determined beforehand. It is worth noting, however, that scan measurements are carried out during the most chaotic period of ablation, before the melt has achieved isotopic equilibrium, which may compromise reproducibility.

In general, there seems to be little prospect of improving the accuracy of $^{206}Pb/^{238}U$ ages using nanosecond laser ablation systems by modelling or other data processing methods. However, design modifications to reduce the size of the ablation chamber and improve transport efficiency might reduce fallback along with Pb/U fractionation and improve sensitivity. Cooling the plasma torch in an oxygen-free environment might also substantially improve sensitivity allowing the use of shallower pits, as would the use of H_2 instead of He for the carrier gas. He has become increasingly expensive and hard to obtain since, unlike Ar, it cannot be recovered from the atmosphere. Obviously, using H_2 would require a fail-safe bypass mechanism to ensure that carrier gas cannot be injected into the plasma before all O_2 has been vented from the ablation chamber.

It is recommended that all published papers where results depend on accurate $^{206}Pb/^{238}U$ ages preserve raw data files (counts or c/s versus time per isotope) in an accessible repository where they can be reprocessed, if necessary, as methods and understanding improve.

https://doi.org/10.5194/egusphere-2026-2779
Preprint. Discussion started: 10 June 2026

Appendix 1: A simple model for U/Pb fractionation during laser ablation

It is assumed that the mass of sample ablated is constant for each pulse (probably not the case for zoned zircon with variable damage) and that the normalized emission profiles for ZrO (NZi) and U (NUi) are specified, where i is the laser pulse number. The normalization factors are the ZrO and U signals that would be measured if there were no loss to the pit or fallback (pulse 0). These are not known but can be no larger than the highest signal and are adjusted to be most consistent with the ratio data.

Fractionation F is defined as $(^{206}Pb/^{238}U)_{cloud,deposit,signal}$ / $(^{206}Pb/^{238}U)_{sample}$ so it will be near 0 in a deposit after most Pb is removed from it, <1 if a new pulse recycles some depleted deposit and >1 in the signal after deposition of Pb-depleted material from the next ablation cloud, provided all of the previous deposit has not been recycled. The Pb loss factor of the deposit, Li, must be specified in the model for each laser pulse i. Li = 0 means no Pb loss while Li = 1 means complete removal of Pb.

First deposit fractionation (pulse 1): $F_{D1} = 1 - L_1$

The proportion of deposit relative to ablated material is quantified by the normalized signal curve for ZrO as $(1 - N_{Z1})$. Its effect on fractionating the first ablation cloud, which produces the measured fractionation, is:

$F_{M1} = 1 + L_1 * (1 - N_{Z1})$, a number that should be slightly greater than 1.

The second ablation cloud may incorporate (recycle) some of the previous deposit. The effect of recycling on the cloud fractionation is quantified by another assigned parameter Ci that varies from 0 (only primary material ablated) to 1 (signal consists entirely of re-ablated deposit). C_1 is 0 since there is no deposit for the first pulse to recycle. The second pulse will ablate new material plus a portion of the previous fractionated deposit in the pit according to the recycling factor C_2. Again, it is assumed that each pulse ablates an equal mass of material. It is also assumed that wall deposits are only momentarily liquid so that material deposited on the wall cannot mix with earlier deposits and is uniquely available for recycling by the following pulse.

If there is recycling, U zoning may affect the $^{206}Pb/^{238}U$ profile because recycled deposit can have a different U concentration from the cloud. For example, if U is increasing this dilutes the effect on the ablation cloud of recycling fractionated deposit because the ablated material has higher U and Pb concentration. The fractionation factor of the ablation cloud from the second pulse after absorbing part of the previous deposit should be:

$F_{A2} = 1 - C_2 * F_{D1} * (1 - N_{Z1}) * (N_{Z2}/N_{U2}) * (N_{U1}/N_{Z1})$

The last two factors represent the ratio of U concentration in the previous deposit to that in the subsequent ablation cloud. These weight the effect of absorbing part of the deposit. This should be a small effect unless U concentration varies rapidly.

https://doi.org/10.5194/egusphere-2026-2779
Preprint. Discussion started: 10 June 2026

The second ablation cloud will form a second deposit depleted according to the assigned second depletion L2 and the fractionation factor of the cloud (F_{A2}, slightly less than 1):

$F_{D2} = (1 – L_2) * F_{A2}$

Formation of this deposit imposes a fractionation on the second ablation cloud, which should normally overcome the effect of partially recycling the previous deposit and be slightly greater than 1.

$F_{M2} = F_{A2} + L_2 * (1 - N_{Z2})$

This is the measured fractionation for the second pulse. Modelled values of normalized $^{206}Pb/^{238}U$ ratios with each successive laser pulse are calculated using these recursive formulas in Supplementary Data File 4 where the general forms are:

Cloud fractionation factor: $F_{Ai} = 1 - Ci * F_{Di–1} * (1 - N_{Zi–1}) * (N_{Zi} / N_{Ui}) * (N_{Ui-1} / N_{Zi-1})$

(after absorbing previous i-1 deposit)

It is assumed that wall deposits are only momentarily liquid after deposition so a new pit deposit can only mix with the previous deposit:

$F_{Di} = (1 – Li) * F_{Ai}$

Note that $N_{Z0} = N_{U0} = F_{D0} = 1$ and $C_1 = 0$ so $F_{A1} = 1$.

https://doi.org/10.5194/egusphere-2026-2779
Preprint. Discussion started: 10 June 2026

References

Butterman, W. C., and Foster, W. R.: Zircon stability and the ZrO2-SiO2 phase diagram. American Mineralogist, 52(5-6), 880-885, 1967.

Caulfield, J. T., Allen, C. M., Ubibe, T., Nguyen, A., and Cathey, H. E.: Compositional heterogeneity in 91500, GJ-1/89 and TEMORA-2 zircon reference materials. Chemical Geology 674, 122580, 2025.

Cottle, J.M., Horstwood, M.S.A. and Parrish, R.R.: A new approach to single shot laser ablation analysis and its application to in situ Pb/U geochronology. J. Anal. At. Spectrom., 24, 1355–1363, https://doi.org/10.1039/b821899d, 2009.

Das, A. and Davis, D.W.: Response of Precambrian zircon to the chemical abrasion (CA-TIMS) method and implications for improvement of age determinations. Geochimica et Cosmochimica Acta, 74, 5333-5348, 2010.

Davis, D.W.: Sub-million-year age resolution of Precambrian igneous events by thermal extraction-thermal ionization mass spectrometer Pb dating of zircon: Application to crystallization of the Sudbury impact melt sheet. Geology 36, 383-386, 2008.

Davis, D. W.: U-Pb geochronology of Archean metasediments in the Pontiac and Abitibi subprovinces, Quebec, constraints on timing, provenance and regional tectonics. Precambrian Research, 115, 97-117, 2002.

Eggins, S. M., Kinsley, L. P. J., and Shelley, J. M. G.: Deposition and element fractionation processes during atmospheric pressure laser sampling for analysis by ICP-MS. Applied Surface Science 127–129, 278–286, 1998.

Gehrels, G. E., Valencia, V. A. and Ruiz, J.: Enhanced precision, accuracy, efficiency, and spatial resolution of U-Pb ages by laser ablation–multicollector–inductively coupled plasma–mass spectrometry, Geochem. Geophys. Geosyst., 9, Q03017, 2008. doi:10.1029/2007GC001805.

https://doi.org/10.5194/egusphere-2026-2779
Preprint. Discussion started: 10 June 2026

Horn, I., Rudnick, R. L., and McDonough, W. F.: Precise elemental and isotope ratio determination by simultaneous solution nebulization and laser ablation-ICP-MS: application to U–Pb geochronology, Chemical Geology, 167, 405-425, 2000.

Jochum, K. P. and 11 others: Determination of Reference Values for NIST SRM 610—617 Glasses Following ISO Guidelines. Geostandards and Geoanalytical Research, 35(4), 397-429, 2011.

Kimura, J.-I., Chang, Q., Itano, K., Iizuka, T., Vaglarov, B., S., and Tani, K.: An improved U–Pb age dating method for zircon and monazite using 200/266 nm femtosecond laser ablation and enhanced sensitivity multiple-Faraday collector inductively coupled plasma mass spectrometry. Journal of Analytical Atomic Spectrometry, 30, 494-505, 2015.

Koch, J. and Günter, D.: Review of the State-of-the-Art of Laser Ablation Inductively Coupled Plasma Mass Spectrometry. Applied Spectroscopy, 65(5), 155A-162A, 2011. doi: 10.1366/11-06255

Kosler, J., Wiedenbeck, M., Wirth, R., Hovorka, J., Sylvester, P. and Mikova, J.: Chemical and phase composition of particles produced by laser ablation of silicate glass and zircon—implications for elemental fractionation during ICP-MS analysis. J. Anal. At. Spectrom., 20, 402–409, 2005.

Kroslakova I. and Gunther, D.: Elemental fractionation in laser ablation-inductively coupled plasma-mass spectrometry: evidence for mass load induced matrix effects in the ICP during ablation of a silicate glass. J. Anal. At. Spectrom., 22, 21-62, 2007. doi: 10.1039/b606522h

May, T. W and Wiedmeyer, R. H.: A Table of Polyatomic Interferences in ICP-MS. Atomic Spectroscopy, 19(5), 150-155, 1998.

Nasdala, L., Kronz, A., Hanchar, J.M., Tichomirowa, M., Davis, D.W. and Hofmeister, W.: Effects of natural radiation damage on back-scattered electron images. American Mineralogist 91, 1739-1746, 2006.

https://doi.org/10.5194/egusphere-2026-2779
Preprint. Discussion started: 10 June 2026

Paton, C., Woodhead, J. D., Hellstrom, J. C., Hergt, J. M., Greig, A. and Maas, R.: Improved laser ablation U-Pb zircon geochronology through robust downhole fractionation correction. Geochemistry, Geophysics, Geosystems, 11, 36p., 2010. doi:10.1029/2009GC002618.

Roberts, N. M. W., Rasbury, E. T., Parrish, R. R., Smith, C. J., Horstwood, M. S. A., and Condon, D. J.: A calcite reference material for LA-ICP-MS U-Pb geochronology: Geochemistry, Geophysics, Geosystems, 18, 2807–2814, 2017. doi.org/10.1002/2016GC006784

Thomas, R.: A Beginner's Guide to ICP-MS – Part 1. Spectroscopy, 16(4), 38-42, 2010.

Thompson, J. M., Meffre, S. and Danyushevsky, L.: Impact of air, laser pulse width and fluence on U–Pb dating of zircons by LA-ICPMS. Journal of Analytical Atomic Spectrometry, 33, 221–230, 2018.

Tomlinson, K.Y., Davis, D.W., Stone, D. et Hart, T.R.: U-Pb age and Nd isotopic evidence for crustal recycling and Archean terrane development in the south-central Wabigoon subprovince, Canada. Contributions to Mineralogy and Petrology, 144, 684-702, 2003.

Wiedenbeck, M. and 8 others: Three natural zircon standards for U-Th-Pb, Lu-Hf, trace element and REE analyses. Geostandards Newsletter 19 (1), 1–23, 1995.

Data availability

Supplementary data files 1 to 8 available through the following link:

https://osf.io/c8j3k/?view_only=f5c96dd8c9244629879f420d5762b74e

Author contributions

DWD is principally responsible for the design of experiments and interpretation of data. HRB carried out measurements and helped with interpretation.

https://doi.org/10.5194/egusphere-2026-2779
Preprint. Discussion started: 10 June 2026

Acknowledgements

Helpful reviews by D. Rubatto, *** are gratefully acknowledged. Some imaging and sample preparation were carried out with Muhammad Nur Aflah Ahmad Zul Kamal. Colin Bray is acknowledged for technical assistance. The authors acknowledge the assistance of Sandra Kamo, director of the Jack Satterly Geochronology Laboratory in providing funding for carrying out the analyses. Laboratory facilities were maintained and made available by Corliss Sio and Colin Bray.